Crystal structure of a multifunctional 2-Cys peroxiredoxin heme-binding protein 23 kDa/proliferation-associated gene product

Shoko Hirotsu*, Yasuko Abe†, Kengo Okada*, Noriyuki Nagahara†, Hiroyuki Hori†, Takeshi Nishino†, and Toshio Hakoshima*‡

*Department of Molecular Biology, Nara Institute of Science and Technology, 8916–5 Takayama, Ikoma, Nara 630-0101, Japan; and †Department of Biochemistry and Molecular Biology, Nippon Medical School, 1-1-5 Sendagi, Bunkyo-ku, Tokyo 113-8602, Japan

Edited by Vincent Massey, University of Michigan Medical School, Ann Arbor, MI, and approved August 13, 1999 (received for review June 11, 1999)

Heme-binding protein 23 kDa (HBP23), a rat isoform of human proliferation-associated gene product (PAG), is a member of the peroxiredoxin family of peroxidases, having two conserved cysteine residues. Recent biochemical studies have shown that HBP23/PAG is an oxidative stress-induced and proliferation-coupled multifunctional protein that exhibits specific bindings to c-Abl protein tyrosine kinase and heme, as well as a peroxidase activity. A 2.6-Å resolution crystal structure of rat HBP23 in oxidized form revealed an unusual dimer structure in which the active residue Cys-52 forms a disulfide bond with conserved Cys-173 from another subunit by C-terminal tail swapping. The active site is largely hydrophobic with partially exposed Cys-173, suggesting a reduction mechanism of oxidized HBP23 by thioredoxin. Thus, the unusual cysteine disulfide bond is involved in peroxidation catalysis by using thioredoxin as the source of reducing equivalents. The structure also provides a clue to possible interaction surfaces for c-Abl and heme. Several significant structural differences have been found from a 1-Cys peroxiredoxin, ORF6, which lacks the C-terminal conserved cysteine corresponding to Cys-173 of HBP23.

Oxidative stress, which is induced by a variety of physiological and pathological conditions, produces reactive oxygen species that damage DNA and most other biological macromolecules. To prevent such cellular damage, living organisms have evolved a defense system involving several antioxidant enzymes, such as superoxide dismutase and catalase, as well as antioxidant molecules such as glutathione and thioredoxin. Oxidative stress also sends signals to the cell nucleus to induce such stress responses as cell-growth arrest and apoptosis. Recently, it has been found that antioxidant proteins have the ability to interact directly with signaling proteins and thereby to control their activity (1–3). One such protein is heme-binding protein 23 kDa (HBP23), which is virtually identical (sequence identities of 95–97%) to human proliferation-associated gene product (PAG) (4), human natural killer cell-enhancing factor A (5), and mouse macrophage stress protein 23 kDa (6). Interestingly, these isoforms have been isolated in association with diverse cellular functions, including proliferation, differentiation, and immune response, as well as oxidative stress. HBP23 was originally identified from rat liver and was shown to have a high binding affinity for heme, which itself may mediate production of reactive oxygen species (7). HBP23/PAG directly binds to a nonreceptor tyrosine kinase, c-Abl (3). The expression of HBP23/PAG is coupled with the cell cycle, as is that of c-Abl, suggesting that high levels of HBP23/PAG expression may counteract the cytostatic activity of c-Abl (8).

HBP23 and its homologues belong to a family of antioxidant enzymes known as peroxiredoxins (Prxs), which show peroxidase activity (9, 10). Prxs are distinct from other peroxidases in that they have no cofactors, such as metals or prosthetic groups. Prxs generally have two conserved cysteines (Cys-52 and Cys-173 of HBP23) at the N- and C-terminal regions (11), and their antioxidant effects are coupled with the physiological electron donor activity of the thioredoxin system (9, 12, 13). A subset of Prxs, 1-Cys Prxs, lacking the C-terminal cysteine, has been reported to exhibit peroxidase activity with DTT as electron donor, although their physiological electron donor has not yet been identified (13). In this paper, we present the crystal structure of a 2-Cys Prx, rat HBP23, and describe the structural basis of the peroxidase activity of Prxs with two cysteines and multifunctional properties that remain largely unclarified.

Materials and Methods

Protein Preparation, Crystallization, and Data Collection. Recombinant HBP23 with the C83S mutation was overexpressed and purified by the methods described previously (14). Approximately 30 mg of native protein and 15 mg of selenomethionyl protein were obtained from a 2-l culture. The samples were concentrated to about 30 mg ml^{-1} after exchanging the buffer for one containing 20 mM Na-phosphate (pH 6.0) and 1 mM 3-[(3-cholamidopropyl)dimethylammonio]-1-propanesulfonate. Crystals suitable for x-ray structural analysis were obtained from a solution mixed with equal volumes of the protein stock solution and a reservoir solution containing 2 M NaCl and 10% polyethylene glycol 6 kDa. These crystals belong to space group $P4_12_12$ ($a = b = 73.9$ Å, $c = 211.3$ Å) and contain one dimer per asymmetric unit. For data collection, radiation-sensitive HBP23 crystals were cryoprotected by soaking them in cryoprotectant containing 10 mM sodium phosphate (pH 6.0), 10% polyethylene glycol 6 kDa, and 3.6 M NaCl. Crystals were then flash frozen to 98 K in a cold nitrogen stream and were maintained at this temperature throughout the data collection. Diffraction data were collected by using an R-AXIS IV imaging-plate area detector (Rigaku, Tokyo) with Cu K_α x-rays generated by a Rigaku FR-C (Tokyo) x-ray generator. Native data sets were collected to 2.6-Å resolution with a completeness of 92.7%. For phase determination, two heavy atom derivatives were prepared by soaking crystals in a solution of 1 mM K_2PtCl_4 and by substitution with selenomethionyl-containing HBP23.

Phasing and Refinement. The diffraction data obtained were processed with DENZO/SCALEPACK (15). The multiple isomorphous replacement phases were calculated with the program SHARP (16) at 3.5-Å resolution and were directly extended to 2.6 Å by means of the solvent-flipping procedure by using the program SOLOMON (17), resulting in a map of sufficient quality to allow tracing of most parts of the molecules. A model was built into the electron density map by using the graphic program O

This paper was submitted directly (Track II) to the PNAS office.

Abbreviations: HBP23, heme-binding protein 23 kDa; PAG, proliferation-associated gene product; Prx, peroxiredoxin; TSA, thiol-specific antioxidant.

Data deposition: The atomic coordinates have be deposited in the Protein Data Bank, www.rcsb.org (PDB ID code IQQ2).

‡To whom reprint requests should be addressed. E-mail: hakosima@bs.aist-nara.ac.jp.

The publication costs of this article were defrayed in part by page charge payment. This article must therefore be hereby marked "*advertisement*" in accordance with 18 U.S.C. §1734 solely to indicate this fact.

Table 1. Statistics of the crystallographic analysis

		Native	K_2PtCl_4 (1)	K_2PtCl_4 (2)	Selenomethionyl protein
Data collection	Resolution, Å	2.6	3.5	3.5	3.2
	Reflections; measured/unique ($I > 1\sigma$)	153,566/18,929	79,148/7,939	57,757/8,035	63,659/10,191
	R_{merge} (the highest shell, %)	7.0 (25.3)	10.3 (19.5)	10.4 (22.0)	9.6 (22.6)
	Completeness (the highest shell) %	92.7 (90.4)	82.6 (74.8)	95.8 (93.6)	86.7 (77.8)
	R_{deri}, %	—	20.4	24.7	21.6
Phasing	Heavy atom site	—	2	2	4
(10 Å–3.5 Å)	Phasing power; acentric/centric	—	2.42/1.68	2.6/2.10	0.89/0.95
	R_{Cullis}; acentric/centric, %	—	0.63/0.60	0.60/0.57	0.92/0.93
Refinement	R_{cryst}/R_{free}, % ($I > 1\sigma$)	21.6/26.8			
(20 Å–2.6 Å)	Mean B factor, Å^2	39.4			
	Protein atoms (solvent/Cl^- ions)	3,478 (62/2)			
	Rmsd bond lengths, Å/angles, °/dihedrals, °/impropers, °	0.018/1.8/26.0/1.8			

K_2PtCl_4 (1), 1 mM K_2PtCl_4 for 6 h; K_2PtCl_4 (2), 1 mM K_2PtCl_4 for 24 h; $R_{sym} = \Sigma |I - \langle I \rangle| / \Sigma I$; $R_{deri} = \Sigma ||F_{PH}| - |F_P|| / \Sigma |F_P|$; phasing power = rms heavy atom structure factor/residual lack of closure; $R_{Cullis} = \Sigma ||F_{PH} - F_P| - |F_{H(calc)}|| / \Sigma |F_{PH} - F_P|$; R_{cryst} and $R_{free} = \Sigma ||F_o| - |F_c|| / \Sigma |F_o|$ where the free reflections (5% of the total used) were held aside for R_{free} throughout refinement.

(18) and refined by several cycles of positional refinement, simulated annealing, and individual B-factor refinement by using X-PLOR (19). Noncrystallographic symmetry restraints were applied during the initial refinement and then relaxed. Throughout the model-building and refinement process, 5% of the reflections were excluded to monitor the R_{free} value. Several cycles of refinements resulted in an R factor of 21.6% and a free R factor of 26.8% against the data from 20.0 Å to 2.6 Å. In the course of the refinement, we observed an electron density too large for a water molecule inside the active site. This peak might be caused by an ion included in the crystallization solution. The positively charged environment suggested that it is probably an anion. The crystallization solution contained two candidates, phosphate ion and chloride ion. However, it was thought that the phosphate ion was too large. Refinement cycles with both possible anions indicated that the peak was probably caused by a chloride ion, which gave a reasonable B factor (32.1 Å^2 for Molecule A and 49.3 Å^2 for Molecule B) close to the averaged B factor (39.4 Å^2). The relatively large B factor of the ion in the Molecule B may indicate partial occupancy, but no refinement of the occupancy was used because of the marginal resolution for this purpose. The final model of the HBP23 dimer includes 346 residues of 398, together with 62 water molecules of which the B factors were smaller than 50 Å. Ribbon representations of the main-chain folding of the protein were drawn by using the programs MOLSCRIPT (20) and QUANTA (Molecular Simulations, Waltham, MA), and the surface representation of the protein was drawn by using the program GRASP (21).

Results

Overall Structure. Recombinant HBP23 with the C83S mutation, which has no effect on the activity but reduces the nature to form aggregates, was crystallized by using NaCl and polyethylene glycol 6 K. The structure was solved by the multiple isomorphous replacement method and refined to an R factor of 21.6% (Table 1). The asymmetric unit of the crystal structure contains one HBP23 dimer. The current structure of HBP23 consists of 173 residues (3–175); the N-terminal 2 and the C-terminal 24 residues (176–199) are not included in the model because of their weak electron densities. Each HBP23 molecule contains six α-helices (α1-α5 and α3′) and seven β-strands (β1-β7) (Fig. 1). The main body comprises a typical thioredoxin fold (22), which contains a central β-sheet (β7, β6, β3, β4) and flanking α-helices (α2, α4, α5). In addition to this fold, a two-stranded β-sheet (β1/β2) and a short α-helix (α1) are added at the N terminus, and two α-helices (α3 and α3′) and a β-strand (β5), which forms a parallel β-sheet with β4, are inserted between β4 and α4. The HBP23 dimer displays a somewhat flattened ellipsoidal shape, with overall dimensions of approximately 60 Å by 40 Å by 25 Å (Fig. 1B). The two molecules (Molecules A and B) of each dimer are related by a 2-fold symmetry and are tightly associated with each other. There is no significant structural difference between the two molecules. The dimer interface buries ≈1,280 Å^2 of solvent-accessible surface per monomer, which amounts to 15% of the total surface of the monomer. The interface is created mainly by the formation of an antiparallel β-sheet (β7 from each monomer) together with several contacts involving the N-terminal loop region, a loop between strand β3 and helix α2 (loop β3-α2), loop α4-β6, and the C-terminal regions containing strand β7, helix α5 and its flanking loops of both ends of the helix. The dimer formation produces a central 10-stranded β-sheet. The interactions at the interface are a mixture of hydrogen bonds, salt bridges, and hydrophobic interactions, as well as van der Waals contacts.

Structural Comparison Between HBP23 and ORF6. Recently, the crystal structure of a 1-Cys Prx, human ORF6, has been determined, and the fundamental framework of its Prx structure and the active site were elucidated (23), although the peroxidase activity and multifunctional properties of 2-Cys Prxs remain largely uncharacterized. The overall topology of HBP23 is similar to that of human ORF6 (28% sequence identity), but several significant differences exist (Fig. 2). ORF6 consists of 224 residues, 21 residues longer than that of HBP23 at the C terminus. ORF6 has an additional C-terminal subdomain that comprises a ≈40-residue segment containing three β-strands and one α-helix. Interestingly, this subdomain partially covers the active site of ORF6. Because of this additional subdomain, the buried interface area (≈1,700 Å^2) of the ORF6 dimer is larger than that of the HBP23. The C-terminal ≈20 residues of HBP23 corresponding to the N-terminal half of this ORF6 subdomain are disordered in the crystal as described. The amino acid sequences of these regions in HBP23 and ORF6 exhibit no homology. In addition, there are two insertion and four deletion sites (Fig. 1C). Superposition of HBP23 and ORF6 gives rms deviations of 3.5 Å for all common 164 C_α atoms and 1.1 Å for 81 selected C_α atoms of common secondary structural elements. The most significant displacements are observed at loop regions β3-α2, α3-β5, α4-β6, and the C-terminal loop, with displacements ranging from 5 Å to over 10 Å. Structural differences are also seen in the common secondary structures. In particular, the long helix α3 of HBP23 is divided into two helices (α3 and α3′)

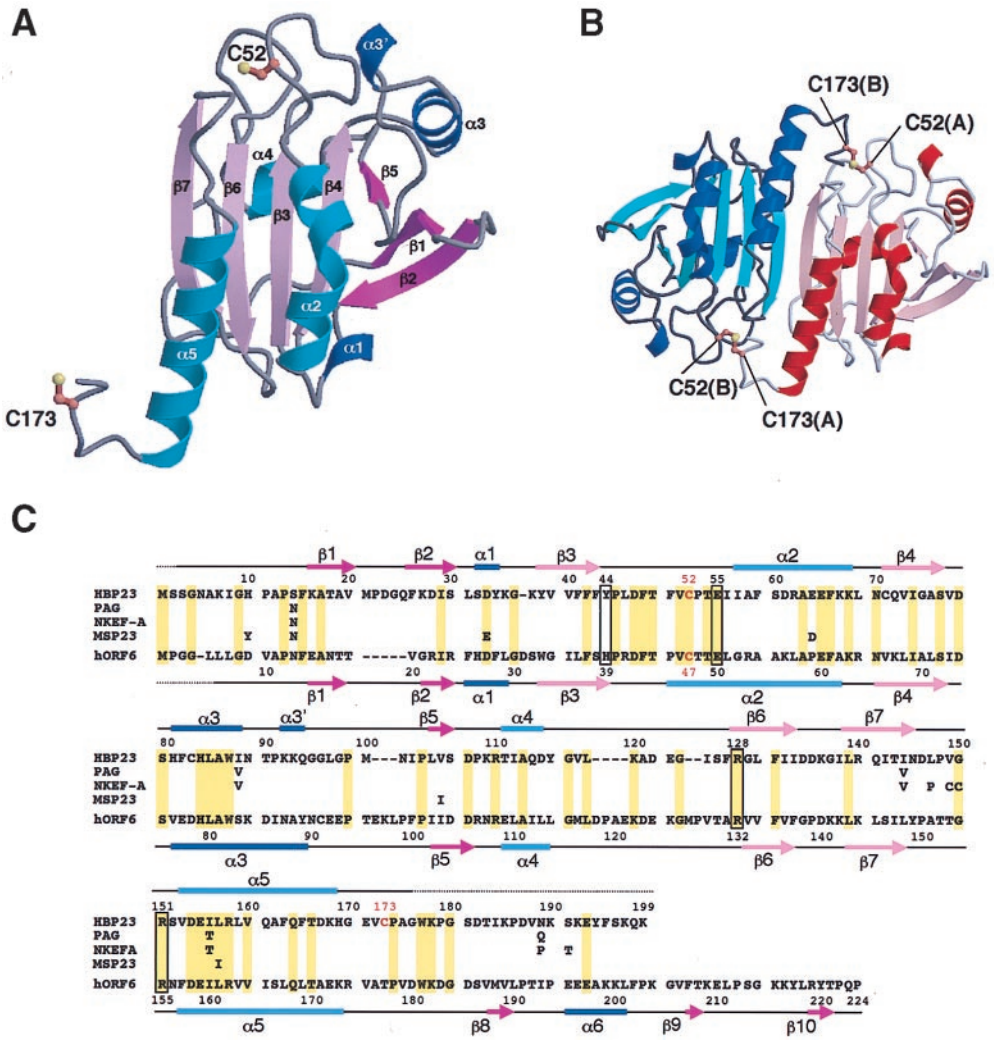

Fig. 1. Overall structure and secondary structural elements of HBP23. (*A*) A ribbon representation of HBP23 showing the secondary structural elements. The α-helices in light blue and β-strands in pale pink form a thioredoxin fold. The other α-helices and β-strands are shown in blue and purple, respectively. The side chains of Cys-52 and Cys-173 are shown with ball-and-stick models. (*B*) A view along the 2-fold axis of the ribbon representation of the HBP23 dimer. The secondary structural elements of Molecule A are shown in red (α-helices) and pale pink (β-strands) and those of Molecule B in blue (α-helices) and sky blue (β-strands). Loop regions of Molecule B are in dark gray. The side chains of two cysteine residues (Cys-52 and Cys-173) at the active site are indicated by ball-and-stick models. (*C*) The secondary structure elements and sequence alignment of HBP23 and the related Prxs. The secondary structural elements of HBP23 and ORF6 are shown (*Top* and *Bottom*, respectively), with the same color codes as in *A*. For the homologues of 2-Cys Prxs (PAG, natural killer cell-enhancing factor A, and mouse macrophage stress protein), substituted residues are shown. Identical residues between HBP23 and ORF6 are highlighted in yellow.

by insertion of proline (Pro-91). Moreover, helix α2 of HBP23 is unwound at the N-terminal part and is bent at Ser-60 because of disruption of the normal α-helix hydrogen bonds. In place of these bonds, the bent site is stabilized by water-mediated hydrogen bonds. This unwinding region of helix α2 and the displaced C-terminal loop contain Cys-52 and Cys-173, respectively. Because the amino acid sequences of the segments around Cys-52 and Cys-173 are fairly homologous with those of ORF6, the conformational differences in these regions may be attributable to formation of the disulfide bond between these two cysteines described below.

Structure of the Active Site. The active site of HBP23 is composed of loops β3-α2 and β7-α5, together with the C-terminal loop of the other molecule of the dimer (Fig. 3*A*). The conserved Cys-52 and Cys-173 are located at loop β3-α2 and the swapped C-terminal loop, respectively. The positions of these active residues are significantly displaced from those of the corresponding residues of ORF6. In particular, the unwinding of helix α2 induces a large displacement of Cys-52 by 6.2 Å from the C_α atom (8.2 Å for the S_γ atom) of the ORF6 active residue Cys-47, which is located at the N-terminal part of the long helix α2. Our sequence alignment indicates Thr-177, but not Val-179, of ORF6 as the corresponding residue of Cys-173 of HBP23 (Fig. 1*C*). The displacement of HBP23 Cys-173 from ORF6 Thr-177 is 4.5 Å (for C_α atoms), which is caused by a conformational change of the C-terminal flanking loop.

Interestingly, the two cysteines, Cys-52 of one HBP23 molecule of the dimer and Cys-173 of the other molecule, form a disulfide bond in the crystal. This oxidized form has been considered an intermediate of the peroxidation reaction catalyzed by 2-Cys Prx members based on *in vitro* experiments (11). The disulfide bond of HBP23 is buried inside the loop and is surrounded by several hydrophobic residues (Fig. 3*B*). The S_γ sulfur atom of Cys-173 is partially exposed to the solvent region, but that of Cys-52, which has been shown to be the active center for the peroxidation of H_2O_2 by mutation analyses (9, 12, 13) (unpublished results), is completely buried. In sharp contrast,

BIOCHEMISTRY

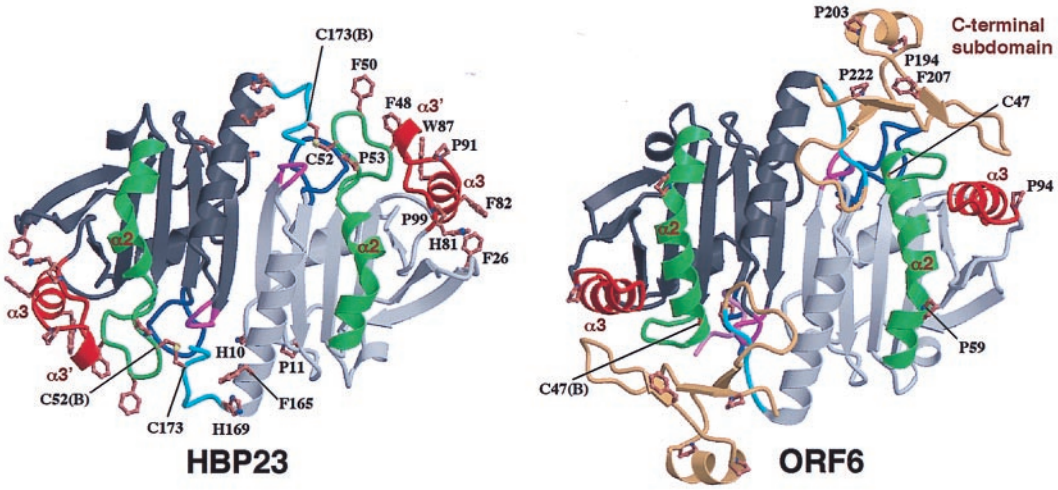

Fig. 2. Structural comparison between HBP23 and ORF6. HBP23 dimer (*Left*) and ORF6 dimer (*Right*) with regions displaying larger displacements highlighted with colors; green for α2 region, red for α3-α3′ region, blue for loop α4- β6, purple for loopβ7-α5, and light blue for the C-terminal tail. The C-terminal subdomain of ORF6 is colored dark yellow. Side chains of two active cysteines (Cys-52 and Cys-173), surface aromatic residues (tryptophan, phenylalanine, histidine), and proline residues are shown.

the active residue Cys-47 of ORF6 was oxidized to cysteine-sulfenic acid (Cys-SOH), an early-stage intermediate in the peroxidation reaction of H_2O_2. It should be noted that the S_γ sulfur atom of ORF6 Cys-47 is located at a narrow pocket that is open to the back side of the molecular surface where HBP23 Cys-173 is exposed. The cysteine sulfenic acid of ORF6 is stabilized by interacting with two positively charged residues, His-39 and Arg-132, as well as a possible Mg^{2+} ion hydrogen-bonded to the sulfenic oxygen atom. It has been proposed that the positively charged environment may stabilize the ionized state of the active site cysteine, lowering its pK_a, and increase the reactivity. His-39 is replaced by Tyr-44 in HBP23 but Arg-132 is conserved in HBP23 (Arg-128) and the other 2-Cys Prxs. Arg-128 of HBP23, however, appears to be located at a considerable distance from Cys-52: the distance between the sulfur atom of Cys-52 and the $N_{\eta 1}$ nitrogen atom of Arg-128 is 7.4 Å (Fig. 3 *A* and *C*). Arg-128 is hydrogen-bonded to conserved Asp-146 and is in close proximity to highly conserved charged residues, Arg-151 and Glu-55. Because both Cys-52 and Cys-173 are located on the flexible loop region, it is possible that, in the reduced form, Cys-52 is located in closer proximity to Arg-128 and Arg-151, where a putative Cl^- ion exists in the present oxidized form and may display enhanced reactivity (nucleophilicity). Superimposing the crystal structure of ORF6 on that of HBP23, the Cl^- ion appears to be very close (1.4 Å) to the position of the sulfur atom of ORF6 Cys-47. Thus, Cys-52 could be located at the position of Cl^- ion in the reduced form. In addition to the positively charged environment, the long helix α5 and the N-terminal part of the bent helix α2 direct their N-terminal ends toward Cys-52, implying stabilization of the charged state of the sulfhydryl group by the helix dipoles.

Discussion

The present crystal structure analysis of rat HBP23 in its oxidized form reveals an unusual structure in which the residue Cys-52 forms a disulfide bond with conserved Cys-173 from another subunit by C-terminal tail swapping. Although HBP23 binds heme with high affinity, as do its homologues (9, 10), this protein can also catalyze H_2O_2 peroxidase heme independently when coupled with the thioredoxin reductase system (data not shown). As in the case of the relatively well characterized *streptococcal* NADH peroxidase (24) and the eukaryotic glutathione peroxidase (25), the cysteine disulfide bond is involved in catalysis via electron transfer between another electron donor component and the disulfide, because in site-directed mutagenesis studies the replacement of either of these cysteines with serine was found to abolish the peroxidase activity with a coupled thioredoxin reductase system (unpublished work). This result also agrees with the mutagenesis studies of yeast thiol-specific antioxidant (TSA) (9), which is a 2-Cys Prx having 59% identities with rat HBP23. In H_2O_2 reduction, Cys-52 presumably yields cysteine-sulfenic acid as the first intermediate as in the cases of yeast TSA (9) and *Salmonella typhimurium* AhpC (26), and this is immediately attacked by Cys-173 to form a disulfide bond and release a molecule of water. In this postulated reaction mechanism, local but significant structural changes should take place around the active site, where, in the reduced form, Cys-52 is accessible to the solvent region to react with peroxide but, in the oxidized form, Cys-52 is buried inside the molecule as described.

The inactivation of HBP23 and TSA by replacement of the C-terminal cysteine by serine seems to be in contrast to the result of the mutagenesis studies of AhpC, where the mutant AhpC lacking the C-terminal cysteine can continue to exhibit its peroxidase activity. Compared with TSA, the homology of this bacterial Prx AhpC with HBP23 is limited to 35% identities: residues located at regions (loop α4-β6, the N-terminal part of helix α2, helices α3-α3′ and the C terminus of helix α5) forming the active site are varied. Moreover, in the case of AhpC, AhpF coupled with NADH was used as the source of reducing equivalents but, in the cases of HBP23 and TSA, thioredoxin was used as the source of reducing equivalents. These differences suggest that the efficiency of reduction of the mutant HBP23 and TSA proteins by the thioredoxin reductase system may not be sufficient to prevent peroxide-mediated inactivation of the mutant proteins. It should be noted that an excess amount of AhpF is needed for the activity of the mutant AhpC protein lacking the C-terminal cysteine.

Like HBP23, the molecular surface of thioredoxin around the active site is largely hydrophobic (22). Thioredoxin has two cysteine residues at the active site, and these residues cycle between two sulfhydryl groups in the reduced form and a disulfide bond in the oxidized form. In both forms of thioredoxin, the active residue Cys-32 is accessible to the solvent region, whereas Cys-35 is almost completely buried. These facts argue that the reduction of HBP23 by thioredoxin may be a

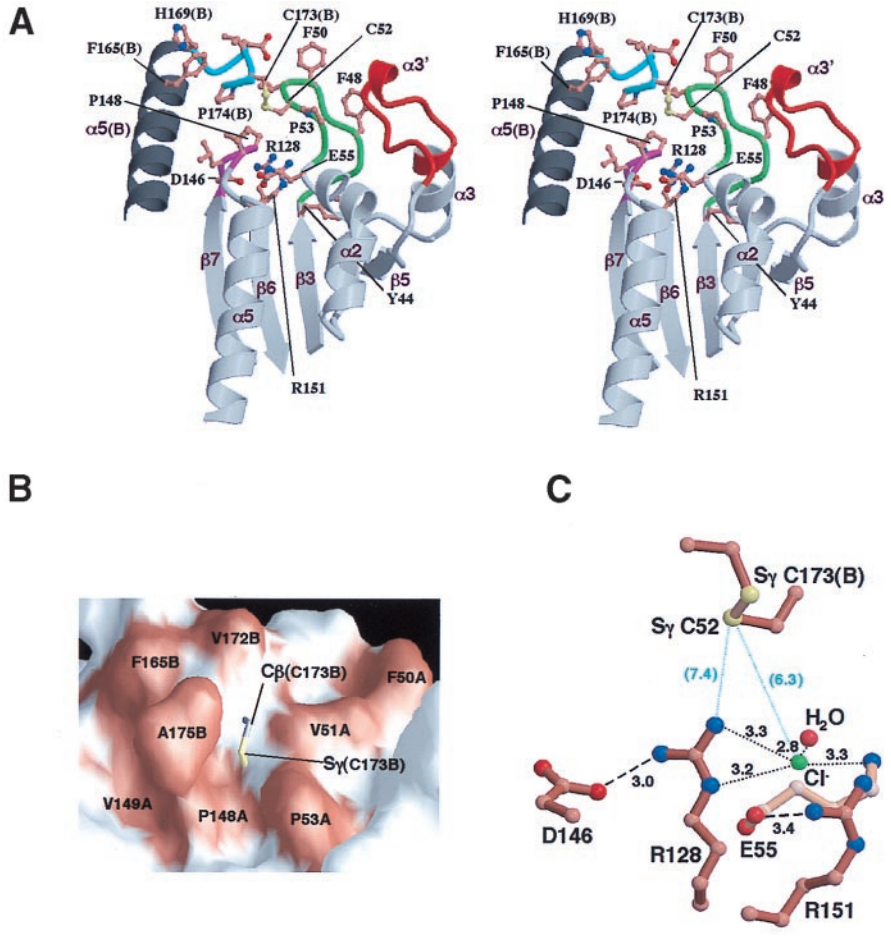

Fig. 3. The active site of HBP23. (*A*) A stereo view of the active site of HBP23. Side chains of Cys-52, Cys-173, and their neighboring residues are shown. Loops are colored as in Fig. 2. (*B*) The accessible molecular surface around the disulfide bond between Cys-52 and Cys-173 at the active site. Cys-173 is represented with a stick model, but Cys-52 is buried inside the molecule. (*C*) A closeup view of the side-chain interactions of the charged residues and a putative Cl^- ion at the bottom of the active site of HBP23. A water molecule contacting the Cl^- ion is observed in Molecule A but is missing in Molecule B.

two-step reaction, in which the first reaction takes place between Cys-173 of HBP23 and Cys-32 of thioredoxin to form a mixed disulfide bond between them, whereas the second reaction breaks the disulfide bond through an attack on Cys-32 by Cys-35 of thioredoxin. The molecular surfaces around thioredoxin Cys-32 and HBP23 Cys-173 show a general shape match, whereas the C-terminal subdomain modifies that of ORF6.

PAG was found to interact specifically with both the c-Abl SH3 and kinase (SH1) domains *in vivo* (3). HBP23/PAG has 12 prolines but lacks the typical proline-rich motif, PXXP, that may bind to the SH3 domain in a polyproline type II (PPII) helical conformation (27, 28). In the current structure, accessible prolines are limited to those at positions 11, 53, 91, and 99 (Fig. 2 *Left*), plus two prolines in the undefined C-terminal tail. Studies with the yeast two-hybrid system have indicated that the C-terminal 79 residues of PAG bind strongly to the c-Abl SH3 domain.

Although the role of heme in this protein is unclear, the binding of HBP23 to heme, with a K_d of 55 nM, is stronger than the binding of HBP23 to porphyrin (210 nM) (7), indicating that a heme iron atom may contribute to the binding in addition to the contribution of the hydrophobic interactions between the porphyrin ring of heme and HBP23. It has also been shown that fluorescence quenching of tryptophan residue(s) is observed when hemin binds to the HBP23 surface (7). HBP23 has two hydrophobic patches, one located around the active site and the other in the region containing helix α3 and loop β1-β2 (Fig. 2 *Left*). Both hydrophobic patches contain histidine residues, His-169 and His-81, respectively, which may interact with the heme iron atom. In addition, Ser-83, which is cysteine in the wild-type protein, is located at helix α3. An exposed tryptophan residue, Trp-87, is located between the two patches. Another tryptophan, Trp-177, is located at the flexible C-terminal loop around the active site. These facts imply that these hydrophobic patches are possible candidates for heme binding.

Thus, the present structure provides a structural basis for the mechanism by which Prxs with two conserved cysteines control antioxidant activity, as well as valuable clues for analyzing the binding sites to the c-Abl SH3 domain and heme.

This work was supported by Grants-in-Aid for Scientific Research (to T.N. and T.H.) and for Scientific Research on Priority Areas of Biometallics (to T.N. and T.H.) from the Ministry of Education, Science, Sports and Culture of Japan. T.H. is a member of the Tsukuba Advanced Research Alliance (TARA Sakabe Project) of Tsukuba University, Tsukuba, Japan.

1. Saitoh, M., Nishitoh, H., Fujii, M., Takeda, K., Tobiume, K., Sawada, Y., Kawabata, M., Miyazono, K. & Ichijo, H. (1998) *EMBO J.* **17,** 2596–2606.
2. Hirota, K., Matsui, M., Iwata, S., Nishiyama, A., Mori, K. & Yodoi, J. (1997) *Proc. Natl. Acad. Sci. USA* **94,** 3633–3638.
3. Wen, S. & Van Etten, R. A. (1997) *Genes Dev.* **11,** 2456–2467.
4. Prosperi, M., Ferbus, D., Karczinski, I. & Goubin, G. (1993) *J. Biol. Chem.* **268,** 11050–11056.
5. Sauri, H., Butterfield, L., Kim, A. & Shau, H. (1995) *Biochem. Biophys. Res.*

Commun. **208**, 964–969.
6. Siow, R. C. M., Ishii, T., Sato, H., Taketani, S., Leake, D. S., Sweiry, J. H., Pearson, J. D., Bannai, S. & Mann, G. E. (1995) *FEBS Lett.* **368,** 239–242.
7. Iwahara, S., Satoh, H., Song, D., Webb, J., Burlingame, A. L., Nagae, Y. & Muller-Eberhard, U. (1995) *Biochemistry* **34,** 13398–13406.
8. Prosperi, M., Ferbus, D., Rouillard, D. & Goubin, G. (1998) *FEBS Lett.* **423,** 39–44.
9. Chae, H. Z., Chung, S. J. & Rhee, S. G. (1994) *J. Biol. Chem.* **269,** 27670–27678.
10. Netto, L. E. S., Chae, H. Z., Kang, S., Rhee, S. G. & Stadtman, E. R. (1996) *J. Biol. Chem.* **271,** 15315–15321.
11. Chae, H. Z., Uhm, T. B. & Rhee, S. G. (1994) *Proc. Natl. Acad. Sci USA* **91,** 7022–7026.
12. Kwon, S. J., Park, J., Choi, W., Kim, I. H. & Kim, K. (1994*) Biochem. Biophys. Res. Comm.* **201**, 8–15.
13. Kang, S. W., Baines, I. C. & Rhee, S. G. (1998) *J. Biol. Chem.* **273,** 6303–6311.
14. Hirotsu, S., Abe, Y., Nagahara, N., Hori, H., Nishino, T., Okada, K. & Hakoshima, T. (1999) *J. Struct. Biol.* **126,** 80–83.
15. Otwinowski, Z. & Minor, W. (1997*) Methods Enzymol.* **276**, 307–326.
16. De la Fortelle, E. & Bricogne, G. (1997) *Methods Enzymol.* **276,** 472–494.
17. Abrahams, J. P. & Leslie, A. G. W. (1996) *Acta Crystallogr.* D **52,** 30–42.
18. Jones, T. A., Zou, J., Cowan, S. W. & Kjeldgaard, M. (1991) *Acta Crystallogr.* A **47,** 110–119.
19. Brunger, A. T., Kuriyan, J. & Karplus, M. (1990) *Acta Crystallogr.* A **46,** 585–593.
20. Kraulis, P. J. (1991) *J. Appl. Crystallogr.* **24,** 946–950.
21. Nicholls, A., Sharp, K. A. & Honig, B. (1991) *Proteins* **11,** 281–296.
22. Weichsel, A., Gasdaska, J. R., Powis, G. & Montfort, W. R. (1996) *Structure (London)* **4,** 735–751.
23. Choi, H., Kang, S. W., Yang, C., Rhee, S. G. & Ryu, S. (1998) *Nat. Struct. Biol.* **5,** 400–406.
24. Poole, L. B. & Claiborne, A. (1989) *J. Biol. Chem.* **264,** 12330–12338.
25. Epp, O., Ladenstein, R. & Wendel, A. (1983) *Eur. J. Biochem.* **133,** 51–69.
26. Ellis, H. R. & Poole, L. B. (1997) *Biochemistry* **36,** 13349–13356.
27. Lim, W. A., Richards, F. M. & Fox, R. O. (1994) *Nature (London)* **372,** 375–379.
28. Pisabarro, M. T., Serrano, L. & Wilmanns, M. (1998) *J. Mol. Biol.* **281,** 513–521.